Variational Structured Attention Networks for Deep Visual Representation Learning

Guanglei Yang, Paolo Rota, Xavier Alameda-Pineda, *Senior Member, IEEE,* Dan Xu, Mingli Ding, Elisa Ricci, *Member, IEEE*

***Abstract*—Convolutional neural networks have enabled major progresses in addressing pixel-level prediction tasks such as semantic segmentation, depth estimation, surface normal prediction and so on, benefiting from their powerful capabilities in visual representation learning. Typically, state of the art models integrate attention mechanisms for improved deep feature representations. Recently, some works have demonstrated the significance of learning and combining both spatial- and channel-wise attentions for deep feature refinement. In this paper, we aim at effectively boosting previous approaches and propose a unified deep framework to jointly learn both spatial attention maps and channel attention vectors in a principled manner so as to structure the resulting attention tensors and model interactions between these two types of attentions. Specifically, we integrate the estimation and the interaction of the attentions within a probabilistic representation learning framework, leading to VarIational STructured Attention networks (VISTA-Net). We implement the inference rules within the neural network, thus allowing for end-to-end learning of the probabilistic and the CNN front-end parameters. As demonstrated by our extensive empirical evaluation on six large-scale datasets for dense visual prediction, VISTA-Net outperforms the state-of-the-art in multiple continuous and discrete prediction tasks, thus confirming the benefit of the proposed approach in joint structured spatial-channel attention estimation for deep representation learning. The code is available at https://github.com/ygjwd12345/VISTA-Net.**

***Index Terms*—probabilistic deep representation learning, semantic segmentation, depth prediction, surface normal estimation**

I. Introduction

OVER the past decade, convolutional neural networks (CNNs) have become the privileged methodology to address computer vision tasks requiring dense pixel-wise prediction, such as semantic segmentation [1], [2], monocular depth prediction [3], [4], contour detection [5] and normal surface computation [6]. Recent studies provided clear evidence that attention mechanisms [7] within deep networks are undoubtedly a crucial factor in improving the performance [1], [5], [2], [8], due to their remarkable effectiveness in enhancing the deep representation learning process. In particular, previous works demonstrated that deeply learned attentions acting as soft weights to interact with different deep features at each channel [9], [10], [11] and at each pixel location [12], [13], [14] permits to improve the pixel-wise prediction accuracy (see Fig.1.(a) and Fig.1.(b)). Recently, Fu et al. [2] proposed the Dual Attention Network (DANet), embedding in a fully convolutional network (FCN) two complementary attention modules, specifically conceived to model separately the semantic dependencies associated to the spatial and to the channel dimensions (Fig.1.(c)).

Concurrently, other approaches have considered the use of attention models integrated within a graph network framework [15], [16], [5], showing the empirical advantage of adopting a graphical model to effectively capture the structured information present in the hidden layers of the neural network and thus enabling the learning of better deep feature representations. Notably, Xu et al. [5], [17] first introduced attention-gated conditional random fields (AG-CRFs), a convolutional neural network implementing a probabilistic graphical model that considers attention variables as gates [18] in order to learn improved deep features and effectively fuse multi-scale information. However, their structured attention model is *only* learned at the spatial level, while channel-wise dependencies are not accounted in their models.

This paper advances research in visual dense representation learning by proposing a novel approach to learn more effective deep representations by integrating a structured attention model which jointly accounts for spatial- and channel-level dependencies using an attention tensor (Fig.1.(d)) within a CRF framework. More precisely, inspired by [5] we model the attention as gates. Crucially, we address the question on how to enforce structure within these latent gates, in order to jointly model spatial- and channel-level dependencies while learning deep features. To do so, we hypothesize that the attention tensor is nothing but the sum of T rank tensors, each of them being the tensor product of a spatial attention map and a channel attention vector. This attention tensor is used as a structured latent attention gate, enhancing the feature maps. We cast the inference problem into a maximum-likelihood estimation formulation that is made computationally tractable thanks to a variational approximation. Furthermore, we implement the maximum likelihood update rules within a neural network, so that they can be jointly learned with the preferred CNN front-end. We called our approach based on structured attention and variational inference VarIational STructured Attention Networks or VISTA-Net. We evaluate our method on multiple pixel-wise prediction problems,

Guanglei Yang and Mingli Ding are with School of Instrument Science and Engineering, Harbin Institute of Technology (HIT), Harbin, China. E-mail:{yangguanglei,dingml}@hit.edu.cn

Xavier Alameda-Pineda is with the Perception Group, INRIA. E-mail: xavier.alameda-pineda@inria.fr.

Dan Xu is with the Department of Computer Science and Engineering, Hong Kong University of Science and Technology. E-mail: danxu@cse.ust.hk.

Paolo Rota and Elisa Ricci are with the Department of Information Engineering and Computer Science, University of Trento, Italy. E-mail: {paolo.rota, elisa.ricci}@unitn.it.

Elisa Ricci is with Deep Visual Learning group at Fondazione Bruno Kessler, Trento, Italy.

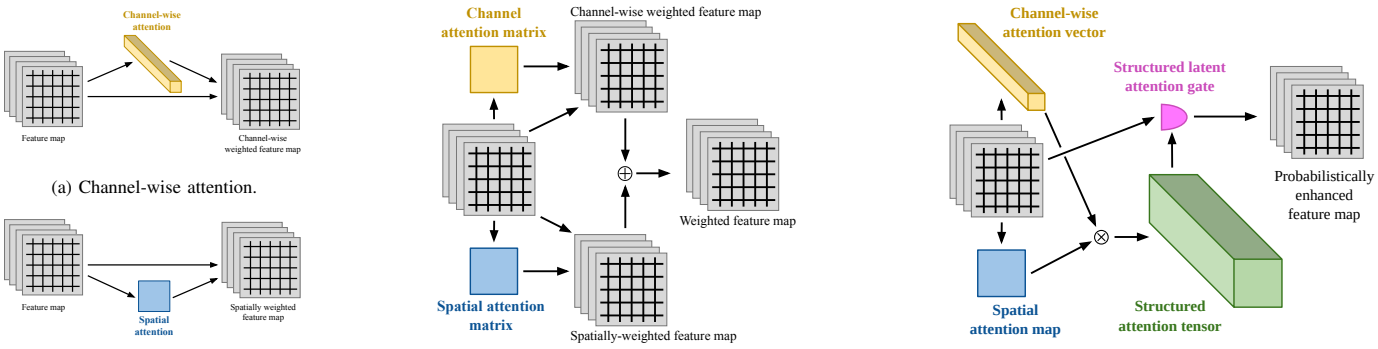

(a) Channel-wise attention.

(b) Spatial attention.

(c) Separate spatial and channel attention.

(d) Proposed structured attention.

Fig. 1: Different attention mechanisms for deep representation learning. (a) and (b) correspond to channel-only and spatial-only attention, respectively. (c) corresponds to previous works [2] combining the spatial- and channel-wise attended representations via simply applying element-wise addition operation $\oplus$ on a spatial and a channel tensor. (d) shows the attention mechanism of VISTA-Net: a channel-wise vector and a spatial map are estimated then tensor-multiplied ($\otimes$) yielding a structured attention tensor. The attention tensor acts as a structured latent gate, producing a probabilistically enhanced feature map.

i.e. monocular depth estimation, semantic segmentation and surface normale prediction, considering six publicly available datasets, *i.e.* NYUD-V2 [19], KITTI [20], Pascal-Context [21], Pascal VOC2012 [22], Cityscape [23] and ScanNet [24]. Our results demonstrate that VISTA-Net is able to learn rich deep representations thanks to the proposed structured attention and to our probabilistic formulation, performing comparably or surpassing state-of-the-art methods.

To summarize, the contribution of this paper is threefold:

- First, we introduce a novel structured attention mechanism for effectively learning deep representations, jointly modeling spatial-wise and channel-wise semantic dependencies and their interactions.
- Second, we propose to use our structured attention tensor within a probabilistic framework, thus introducing a principled manner of modeling the statistical relationships between channel-wise and spatial-wise attention.
- Third, extensive experiments are conducted on three distinct pixel-wise prediction tasks and on six different challenging datasets, demonstrating that the proposed framework is competitive or outperforms previous methods while being task-agnostic, i.e. applicable to different continuous and discrete pixel-level prediction problems.

II. Related Work

In this section we review previous works on three important pixel-wise prediction tasks, *i.e.* monocular depth estimation, semantic segmentation and surface normal prediction, on which the effectiveness of our approach is extensively demonstrated. As our key contribution is the introduction of a novel variational structured attention mechanism, we also discuss previous works considering attention models for deep representation learning.

A. Pixel-wise Prediction

Monocular Depth Estimation. Most recent works on monocular depth estimation are based on CNNs [25], [3], [26], [4], [27], [28], [29], [30]. For instance, Eigen *et al.* [6] introduced a two-streams deep network to take into account both coarse global prediction and local information. Fu *et al.* [28] proposed a discretization strategy to treat monocular depth estimation as a deep ordinal regression problem. They also employed a multi-scale network to capture relevant multi-scale information. Lee *et al.* [30] introduced local planar guidance layers in the network decoder module to learn more effective features for depth estimation. More recently, PackNet-SfM [31] used 3D convolutions with self-supervision to learn detail-preserving representations.

Our approach is related to previous works using CRF for depth estimation. Wang *et al.* [26] introduced a two-layer hierarchical CRF to fuse global and region-wise local predictions. Another related work to ours is [3], which proposed an end-to-end trainable network implementing a continuous CRF. Xu *et al.* [32] improved over [3] by presenting a multi-scale continuous CRF model to learn the multi-scale features and optimally fuse them. More recently, Xu *et al.* [17] proposed the AG-CRF model, incorporating spatial dependencies within a structured probabilistic framework. Our approach significantly differ from these previous methods as it incorporates spatial- and channel-wise dependencies within a single attention tensor and integrates it in a CRF framework.

Semantic Segmentation. As for depth estimation, nowadays CNNs are the mainstream approach for semantic segmentation. Long *et al.* [33] were the first to introduce fully convolutional networks (FCNs) for semantic segmentation, achieving significant improvements over previous models. Dilated convolutions [34], [35] were designed in order to increase the receptive field while learning deep representations, further boosting performances. OCNet [36] introduced a context aggregation strategy, *i.e.* object context pooling, for robust segmentation. In APCNet [37] multi-scale contextual representations were constructed with multiple Adaptive Context Modules. Other works focused on multi-scale feature representation learning, designing appropriate convolutional encoder-decoder network structures [38], [39] or considering end-to-end trainable archi-

tectures modeling CRFs [40], [41], [42]. Our approach also adopts a probabilistic graphical model formulation but it is the first which jointly models structured spatial- and channel-wise semantic dependencies.

Surface Normal. Extracting 3D geometry from a single image is a longstanding problem in computer vision. Surface normal estimation is a classical task in this context, which requires modeling both global and local features. Typical approaches leverage on networks with high capacity to achieve accurate predictions at high resolution. For instance, FrameNet [43] employed the DORN [28] architecture, a modification of DeepLabv3 [34] that removes multiple spatial reductions (2×2 max pool layers), to generate high resolution surface normal maps. A different strategy consists in designing appropriate loss terms. For instance, UprightNet [44] considered an angular loss and showed its effectiveness for the task. Unlike previous works focusing on designing *ad hoc* network structures or proposing new loss terms, here we show that introducing a structured attention module into a deep network is effective for surface normal prediction.

Some existing works extended joint deep learning of dense pixel-wise prediction tasks [45], [46], [47], [48], [49], [17], [50]. Such as, Xu *et al.* [45] designed a PAD-Net architecture that learns multiple auxiliary pixel-wise tasks and presents a multi-task distillation module to combine the predictions from the different auxiliary tasks to help more critical final tasks. Moreover, Vandenhende and Van Gool *et al.* [49] further improved PAD-Net by introducing multi-scale multi-modal distillation propagating distilled task information from lower to higher scales. However, these works are focusing more on practical design for learning interaction between different pixel-wise tasks. At the same time, our model targets a variational structured attention network for multi-scale feature fusion, which could provide a theoretic explanation. Thus, it has clear benefit for a more effective deep module design.

B. Attention Models

Several works have considered integrating attention models within deep architectures to improve performance in several tasks such as image categorization [51], speech recognition [52] and machine translation [53], [54], [55]. Focusing on pixel-wise prediction, Chen *et al.* [1] first described an attention model to combine multi-scale features learned by a FCN for semantic segmentation. Zhang *et al.* [10] designed EncNet, a network equipped with a channel attention mechanism to model global context. Zhao *et al.* [56] proposed to account for pixel-wise dependencies introducing relative position information in spatial dimension within the convolutional layers. Huang *et al.* [57] described CCNet, a deep architecture that embeds a criss-cross attention module with the idea of modeling contextual dependencies using sparsely-connected graphs, such as to achieve higher computational efficiency. Fu *et al.* [2] proposed to model semantic dependencies associated with spatial and channel dimensions by using two separate attention modules. Zhong *et al.* [9] introduced a squeeze-and-attention network (SANet) specialized to pixel-wise prediction taking into account spatial and channel inter-dependencies in an efficient way.

Attention was first adopted within a CRF framework by [5], which introduced gates to control the message passing between latent variables and showed that this strategy is effective for contour detection. PGA-Net [17] improved over this work proposing feature dependant conditional kernels. Our work significantly departs from these approaches, as we introduce a novel structured attention mechanism, jointly handling spatial- and channel-level dependencies within a probabilistic framework. Notably, we also prove that our model can be successfully employed in case of several challenging dense pixel-level prediction tasks, where it significantly outperforms both AG-CRF [5] and PGA-Net [17].

Our work is also closely related to previous studies on dual graph convolutional network [58] and dynamic graph message passing networks [15], which have been successfully used for pixel-level prediction tasks. However, while they also resort on message passing for learning refined deep feature representations, they lack a probabilistic formulation. Finally, previous studies [32], [41], [16] described CRF-based models for pixel-wise estimation, *e.g.* to learn and optimally fuse deep representations at multiple scales. However, they did not employ structured attention gates.

III. Variational Structured Attention Networks

As previously discussed, the goal of our work is to enhance the learned representation by structuring the attention within a probabilistic formulation. On the one side, inducing structure in the attention mechanisms has been proven to be successful [2], [9]. On the other side, probabilistic formulations combined with deep architectures are interesting for pixel-level prediction tasks [59]. Up to our knowledge, we are the first to bring together recent advances in pixel-wise prediction by formulating a novel structured attention mechanism within a probabilistic CRF-like inference framework. In the following, we first describe the problem formulation, and specifically how to structure the attention within a CRF formulation. Secondly, we derive the energy function as well as the variational approximation. Finally, the derived inference formulae and associated algorithm are detailed.

A. Problem Formulation

Given an input image $\mathbf{I}$, we consider a generic front-end CNN model with parameters θ_c, which outputs a set of S multi-scale feature maps $\mathbf{F} = \{\mathbf{f}_s\}_{s=1}^{S}$. To each of these feature maps (or scale) s, we can associate a hidden feature map $\mathbf{z}_s$ of the same size of $\mathbf{f}_s$, and that needs to be inferred within the CRF formulation. These hidden variables correspond to refined convolutional futures that incorporate information and attention from other feature maps, so as to better represent the key information for the pixel-level task at hand. For each pair of *emitting* e and *receiving* r feature maps, we associate the usual CRF pair-wise kernel, denoted by $\mathbf{k}_r^e$ as well as an attention tensor $\mathbf{a}_r^e$. This attention tensor should encode the entries of the emitting feature map that better help the inference of the receiving hidden features. Indeed, we inspire from the CRF formulation with gating variables proposed in [5], so that each entry of the attention tensor is a

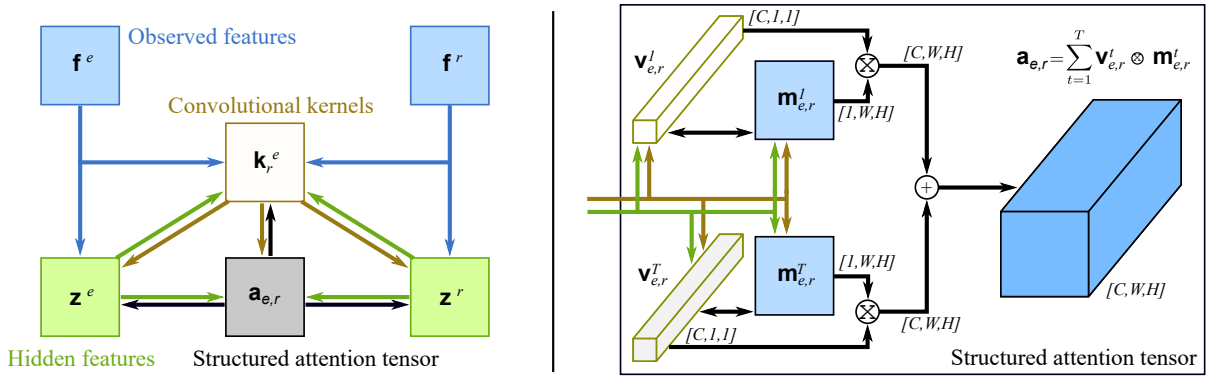

Fig. 2: Schematic representation of the various hidden variables in VISTA-Net. (left) For each pair of emitting e and receiving r scales, their respective convolutional features $\mathbf{f}$ are shown in blue, their hidden variables $\mathbf{z}$ in green, the associated learned kernel $\mathbf{k}$ in yellow, and the channel-wise and spatial attention vector and matrix $\mathbf{v}$ and $\mathbf{m}$ in red. Arrows of the corresponding color denote the flow of information when updating the variable. (right) The computational relationships between the channel-wise and spatial attention variables is shown, as well as the operations required to compute the final structured attention tensor $\mathbf{a}$.

binary variable indicating whether or not the emitting feature map entry should be used to infer the receiving feature map entry.

Inspired by [2], where a spatial- and a channel-wise *full-rank* tensors are computed, we opt to infer different spatial and channel attention variables. Differently from [2], we propose to structure a generic attention tensor $\mathbf{a}$ (we drop the emitting and receiving scale indices for now) of dimension $W \times H \times C$ (widht, height, channels), as the sum of T rank-1 tensors, as shown in Fig.2 (right), by writing:

$$\mathbf{a} = \sum_{t=1}^{T} \mathbf{m}^t \otimes \mathbf{v}^t \in \{0,1\}^{W \times H \times C}, \tag{1}$$

where $\mathbf{m}^t$ is a binary image of $P = W \times H$ pixels, $\mathbf{m}_t \in \{0,1\}^P$, and $\mathbf{v}^t$ is a stochastic vector of dimension C, $\mathbf{v}^t \in \{0,1\}^C$, $\sum_{c=1}^{C} v^{t,c} = 1$, and $\otimes$ denotes the tensor product, in the case above leading to a 3-way binary tensor of dimensions $W \times H \times C$. Each of the tensor products within the sum yields a tensor of rank-1, consequently limiting the rank of $\mathbf{a}$ to be at maximum T. In this way, we reduce ambiguity and ease the learning. This also means that the model is conceived to pay attention to only T channels of the feature map. While this could seem limiting at first glance we remark that: (i) the model learns which are the *optimal* T channels among the possible C that have to be used to refine the hidden variables and (ii) the a posteriori distribution of $\mathbf{m}^t$ boils down to a convex combination of all channels, as it will appear clear when discussing the inference procedure. (1) is the algebraic expression of the proposed structured attention mechanism, and is the methodological foundation of VISTA-Net. Intuitively, the structured attention tensor should help refining the hidden variables $\mathbf{z}_s$ to allow better performance at various pixel-level prediction tasks.

For each emitting-receiving pair of scales, e and r, we thus propose to infer the T associated attention maps $\{\mathbf{m}^t_{e,r}\}_{t=1}^T$ and vectors $\{\mathbf{v}^t_{e,r}\}_{t=1}^T$, structuring the attention tensors. In addition, we also propose to learn the pair-wise binary kernels of the CRF, $\mathbf{k}^e_r$. We believe learning the kernels is important because it allows the CRF to weight the information flow depending on the content of the rather than keeping the same weights for all images.

Summarizing, in addition to the set of hidden CRF feature maps, $\mathbf{Z} = \{\mathbf{z}_s\}_{s=1}^S$, we propose to infer the set of pair-wise CRF kernels $\mathbf{K} = \{\mathbf{k}^e_r\}_{e,r}^{S,S}$ and the sets of spatial-wise and channel-wise attention maps and stochastic vectors, denoted as $\mathbf{M} = \{\mathbf{m}^t_{e,r}\}_{e,r,t=1}^{S,S,T}$ and $\mathbf{V} = \{\mathbf{v}^t_{e,r}\}_{e,r,t=1}^{S,S,T}$, respectively. In the following section, we describe the energy function associated to our formulation and propose a variational approximation that allows us to derive closed-form solutions for the a posteriori distributions of all the aforementioned random variables.

B. Energy Function and Variational Approximation

Our model consists on three different latent variables: the hidden features $\mathbf{Z}$, and the hidden attention maps $\mathbf{M}$ and vectors $\mathbf{V}$. In addition, we also consider inferring the CRF kernels, denoted by $\mathbf{K}$ from the data. More precisely, the energy function associated to the proposed models writes:

$$\begin{aligned} -E(\mathbf{Z},\mathbf{M},\mathbf{V},\mathbf{K},\mathbf{F},\Theta) &= \sum_s \sum_{p,c} \phi_z(z_r^{p,c}, f_r^{p,c}) \\ &+ \sum_{e,r} \sum_{p,c,p',c'} \sum_t m^{t,p}_{e,r} v^{t,c}_{e,r} \psi(z_r^{p,c}, z_e^{p',c'}, k^{e,p',c'}_{r,p,c}) \\ &+ \phi_k(f_r^{p,c}, f_e^{p',c'}, k^{e,p',c'}_{r,p,c}). \end{aligned} \tag{2}$$

where ϕ_z, ϕ_k and ψ are potentials to be defined and $k^{e,p',c'}_{r,p,c}$ denotes the kernel value weighting the information flow from the (p',c')-th value of the feature map of scale e to the (p,c)-th value of the feature map of scale r. Since the exact a posteriori distribution is not computationally tractable, we opt to approximate it with the following family of separable distributions:

$$\begin{aligned} p(\mathbf{Z},\mathbf{M},\mathbf{V},\mathbf{K}|\mathbf{F},\Theta) &\approx q(\mathbf{Z},\mathbf{M},\mathbf{V},\mathbf{K}) \\ &= q_z(\mathbf{Z}) q_m(\mathbf{M}) q_v(\mathbf{V}) q_k(\mathbf{K}). \end{aligned} \tag{3}$$

In that case, the optimal solution for each of the factors of the distribution is to take the expectation w.r.t. to all the others, for instance:

$$q_z(\mathbf{Z}) \propto \exp\Big(-\mathbb{E}_{q_m(\mathbf{M})q_v(\mathbf{V})q_k(\mathbf{K})}\Big\{E(\mathbf{Z},\mathbf{M},\mathbf{V},\mathbf{K},\mathbf{F},\Theta)\Big\}\Big). \tag{4}$$

It can be shown that the optimal variational factors write:

$$\begin{aligned}
q_z(z_r^{p,c}) &\propto \exp\Big(\phi_z(z_r^{p,c}, f_r^{p,c}) \\
&\quad + \sum_{e\neq r}\sum_t \bar{m}_{e,r}^{t,p}\bar{v}_{e,r}^{t,c}\sum_{p',c'}\mathbb{E}_{q_z q_k}\{\psi(z_r^{p,c}, z_e^{p',c'}, k_{r,p,c}^{e,p',c'})\}\Big),\\
q_m(m_{e,r}^{t,p}) &\propto \exp\Big(m_{e,r}^{t,p}\sum_c \bar{v}_{e,r}^{t,c}\sum_{p',c'}\mathbb{E}_{q_z,q_k}\{\psi(z_s^{p,c}, z_{s'}^{p',c'}, k_{r,p,c}^{e,p',c'})\}\Big),\\
q_v(v_{e,r}^{t,c}) &\propto \exp\Big(v_{e,r}^{t,c}\sum_p \bar{m}_{e,r}^{t,p}\sum_{p',c'}\mathbb{E}_{q_z,q_k}\{\psi(z_s^{p,c}, z_{s'}^{p',c'}, k_{r,p,c}^{e,p',c'})\}\Big),\\
q_k(k_{r,p,c}^{e,p',c'}) &\propto \exp\Big(\phi_k(f_r^{p,c}, f_e^{p',c'}, k_{r,p,c}^{e,p',c'}) \\
&\quad + \sum_t \bar{m}_{e,r}^{t,p}\bar{v}_{e,r}^{t,c}\mathbb{E}_{q_z}\{\psi(z_s^{p,c}, z_{s'}^{p',c'}, k_{r,p,c}^{e,p',c'})\}\Big).
\end{aligned}$$

where $\bar{m}_{e,r}^{t,p} = \mathbb{E}_{q_m}\{m_{e,r}^{t,p}\}$ denotes the a posteriori mean, and analogously for $\bar{v}_{e,r}^{t,c}$. This result also implies that thanks to the variational approximation in (3), the posterior distributions factorise in each of the variables above, *e.g.* $q_z(\mathbf{Z}) = \prod_{r,p,c=1}^{S,P,C} q_z(z_r^{p,c})$.The relation between the various hidden variables as for their inference is shown in Fig.2 (left). In addition, we also show the information flow between the hidden variables using arrows. Finally, in Fig.2 (right) we show the relation between the channel-wise and spatial attention variables and how the final structured attention tensor is computed.

C. Inference with VISTA-Net

In order to construct an operative model we need to define the potentials ϕ_z, ϕ_k and ψ. In our case, the unary potentials correspond to:

$$\begin{aligned}
\phi_z(z_r^{p,c}, f_r^{p,c}) &= -\frac{b_r^{p,c}}{2}(z_r^{p,c} - f_r^{p,c})^2,\\
\phi_k(f_r^{p,c}, f_e^{p',c'}, k_{r,p,c}^{e,p',c'}) &= -\frac{1}{2}(k_{r,p,c}^{e,p',c'} - f_r^{p,c} f_e^{p',c'})^2.
\end{aligned} \tag{5}$$

where $b_s^{p,c} > 0$ is a weighting factor. ψ is bilinear in the hidden feature maps:

$$\psi(z_r^{p,c}, z_e^{p',c'}, k_{r,p,c}^{e,p',c'}) = z_r^{p,c} k_{r,p,c}^{ep',c'} z_e^{p',c'}. \tag{6}$$

Using the over bar notation also for the hidden features and kernels, e.g. $\bar{z}_s^{p,c} = \mathbb{E}_{q_z}\{z_s^{p,c}\}$, and by combining the kernel definitions (5) and (6) with the expression of the variational factors (5), we obtain the following update rules for the latent variables.

Z-step. It can be seen that the posterior distribution on q_z is Gaussian with mean:

$$\bar{z}_s^{p,c} = \frac{1}{b_s^{p,c}}\Big(b_s^{p,c} f_s^{p,c} + \sum_e\sum_t \bar{m}_{s,s'}^{t,p}\bar{v}_{s,s'}^{t,c}\sum_{p',c'}\bar{k}_{r,p,c}^{e,p',c'}\bar{z}_{s'}^{p',c'}\Big) \tag{7}$$

This corresponds to the update rule obtained in [5] with two remarkable differences. First, the posterior of the attention gate corresponds to the posterior of the structured tensor of rank T. Second, the impact of the neighboring features is weighted by the expected kernel value $\bar{k}_{r,p,c}^{e,p',c'}$.

M-step. The variational approximation leads to a Bernoulli distribution for $q_m(m_{e,r}^{t,p})$, which boils down to the following a posteriori mean value using the sigmoid function σ:

$$\bar{m}_{e,r}^{t,p} = \sigma\Big(\sum_c \bar{v}_{e,r}^{t,c}\sum_{p',c'}\bar{z}_s^{p,c}\bar{k}_{r,p,c}^{e,p',c'}\bar{z}_{s'}^{p',c'}\Big). \tag{8}$$

V-step. It can be shown that the approximated posterior distribution is categorical, and that the expected value of each dimension of $\mathbf{v}_{e,r}^t$ can be computed using the softmax operator:

$$(\bar{v}_{e,r}^{t,c})_{c=1}^C = \text{softmax}\Big(\sum_p \bar{m}_{e,r}^{t,p}\sum_{p',c'}\bar{z}_s^{p,c}\bar{k}_{r,p,c}^{e,p',c'}\bar{z}_e^{p',c'}\Big)_{c=1}^C. \tag{9}$$

K-step. Finally, we need to derive the update rules for $\mathbf{K}$. By further deriving the corresponding variational posterior distribution, it can be shown that the a posteriori distribution for the kernels is a Gaussian distribution with the following mean:

$$\bar{k}_{r,p,c}^{e,p',c'} = f_r^{p,c} f_e^{p',c'} + \sum_t \bar{m}_{e,r}^{t,p}\bar{v}_{e,r}^{t,c}\bar{z}_r^{p,c}\bar{z}_e^{p',c'}. \tag{10}$$

This solution is very straightforward, but since the kernels are estimated independently for each pair of receiving (r,p,c) - emitting (e,p',c') pixels, it has two major drawbacks. First, the kernel values are estimated without any spatial context. Second, given the large amount of kernel values, one must find a very efficient way to compute them. We propose to kill two birds with one stone by learning the kernels from the features using convolutional layers. By design, they take spatial context into account, and many popular libraries have efficient implementations of the convolution operation. The estimated kernel corresponding to the input channel c' of scale e, $\mathbf{k}_r^{e,c'}$ is computed via a convolutional operation. The input of the convolution is a concatenation of the tensor $\mathbf{f}_r + \mathbf{z}_r \sum_{t=1}^T \bar{m}_{r,e}^t \otimes \bar{v}_{r,e}^t$ and the image $\mathbf{z}_e^{c'}$ resized to the spatial size of $\mathbf{f}_r$.

Joint Learning. We implement the inference procedure described before within the neural network, on the top of the CNN front-end. Indeed, implementing all inference operations using available deep learning operators has two prominent advantages. First, we can perform the inference and learning the CNN front-end at the same time, within the same formalism and for the same aim. Second, this allows direct parallelisation of our method, speeding up training and inference.

The precise implementation goes as follows. Regarding $\bar{\mathbf{z}}_r$, we first apply message passing from the e-th scale to the r-th scale is performed with $\mathbf{z}_{e\to r} \leftarrow \bar{\mathbf{k}}_r^e \circledast \bar{\mathbf{z}}_e$, where $\circledast$ denotes the convolutional operation and $\bar{\mathbf{k}}_r^e$ denotes the corresponding learned convolution kernel. We then apply element-wise product with the corresponding structured attention tensor $\sum_{t=1}^T \bar{\mathbf{m}}_{e,r}^t \otimes \bar{\mathbf{v}}_{e,r}^t$. Finally we compute the element-wise sum with other emiting scales and the feature maps $\mathbf{f}_r$, see (7). Regarding $\bar{\mathbf{m}}_{e,r}$, we first compute the element-wise product between $\bar{\mathbf{z}}_r$ and $\mathbf{z}_{e\to r}$. The sum over channels weighted by $\bar{\mathbf{v}}_{e,r}$ is computed previous to applying pixel-wise sigmoid,

Algorithm 1: Our VISTA-Net for a given receiving scale r.

Input :
- $\{\mathbf{f}_e\}_{e\in E}$ – set of emitting feature map.
- $\mathbf{f}_r$ – receiving feature map.

Output:
- $\hat{\mathbf{f}}_r$ – updated receiving feature map.

for $e \in E$ **do**
  $\bar{\mathbf{z}}_e \leftarrow \bar{\mathbf{k}}_r^e \circledast \mathbf{f}_e$
  $\bar{\mathbf{z}}_{e\to r} \leftarrow \bar{\mathbf{k}}_r^e \circledast \bar{\mathbf{z}}_e$ – will replace $\mathbf{z}_{s'}$ in (5)-(10).
end for
$\bar{\mathbf{z}}_r \leftarrow \mathbf{b}_r^{-1}\Big(\mathbf{b}_r \odot \mathbf{f}_r + \sum_e \bar{\mathbf{z}}_{e\to r} \odot \sum_t \bar{\mathbf{m}}_{r,e}^t \otimes \bar{\mathbf{v}}_{r,e}^t\Big)$
(where $\mathbf{b}_r^{-1}$ denotes the element-wise inverse)
for $t \leftarrow 1$ **to** T **do**
  $\mathbf{m}_{r,e}^t \leftarrow \sum_c \bar{v}_{r,e}^{t,c} \left(\bar{\mathbf{z}}_r \odot \bar{\mathbf{z}}_{e\to r}\right)_c$
  (where $()_c$ extracts the c-th channel)
  $\bar{\mathbf{m}}_{r,e}^t \leftarrow \text{sigmoid}(\mathbf{m}_{r,e}^t)$
  $\mathbf{v}_{r,e}^t \leftarrow \sum_p \bar{m}_{r,e}^{t,p} \left(\bar{\mathbf{z}}_r \odot \bar{\mathbf{z}}_{e\to r}\right)^p$
  (where $()^p$ extracts the p-th pixel)
  $\bar{\mathbf{v}}_{r,e}^t \leftarrow \text{softmax}(\mathbf{v}_{r,e}^t)$
end for
$\bar{\mathbf{k}}_r^e \leftarrow \mathbf{f}_r \otimes \mathbf{f}_e + \left(\sum_t (\bar{\mathbf{m}}_{r,e}^t \otimes \bar{\mathbf{v}}_{r,e}^t) \odot \bar{\mathbf{z}}_r\right) \otimes \bar{\mathbf{z}}_e$
$\hat{\mathbf{f}}_r \leftarrow \mathbf{f}_r + \bar{\mathbf{z}}_r \odot \sum_t \bar{m}_{r,e}^t \otimes \bar{v}_{r,e}^t$
return $\hat{f}_r$

see (8). Regarding $\bar{\mathbf{v}}_{e,r}$ we operate in a very similar fashion, but weighting each pixel with $\bar{\mathbf{m}}_{e,r}$ and then summing every channel independently, before applying softmax, see (9). Regarding $\bar{\mathbf{k}}_r^{e,c'}$, as discussed before, it is computed via a convolutional operation on the concatenations of $\mathbf{f}_{t_m} + \mathbf{g}_{t_m}$ and the image $\mathbf{z}_e^{c'}$ resized to the spatial size of $\mathbf{f}_r$. In terms of initialisation, we draw a random guess for $\mathbf{M}$ and $\mathbf{V}$, and set $\mathbf{Z}$ to $\mathbf{F}$. This allows us to update the kernels, then the other variables. Our structured attention method is summarised in Algorithm 1.

Once the hidden variables are updated, we use them to address several different pixel-wise prediction tasks involving continuous and discrete variables, including monocular depth estimation, surface normal estimation and semantic segmentation. Following previous works, the network optimization losses for these three tasks are a standard L2 loss [32], a cosine similarity loss [6] and a cross-entropy loss [34], respectively. The CNN front-end and VISTA-Net, are jointly trained end-to-end.

IV. Experimental Evaluation

A. Datasets

The NYU-v2 dataset [19] is used to evaluate our approach in the depth estimation task. We use 120K RGB-Depth pairs with a resolution of 480×640 pixels, acquired with a Microsoft Kinect device from 464 indoor scenes. We follow the standard train/test split as previous works [6], using 249 scenes for training and 215 scenes (654 images) for testing.

The KITTI dataset [20] is a large-scale outdoor dataset created for various autonomous driving tasks. We use it to evaluate the depth estimation performance of our proposed model. Following the standard training/testing split proposed by Eigen *et al.* [6], we specifically use 22,600 frames from 32 scenes for training, and 697 frames from the rest 29 scenes for testing.

The Pascal-Context dataset [21] is used for assessing the performance of VISTA-Net on the semantic segmentation task. It consists of RGB images from Pascal VOC 2010 and annotated semantic labels for more than 400 classes. As in previous works [34], [10], we consider the most frequent 59 classes plus the background class. The remaining classes are masked during training and testing.

The PASCAL VOC2012 dataset [22] is the most widely studied segmentation benchmark, which contains 20 classes and is composed of 10582 training images, and 1449 validation images, 1456 test images. We train the VISTA-Net using augmented data as previous works [9], [33].

The Cityscapes dataset [23] is tasked for urban segmentation, Only the 5,000 finely annotated images are used in our experiments and are divided into 2,975/500/1,525 images for training, validation, and testing.

The ScanNet dataset [24] is a large RGB-D dataset for 3D scene understanding. We employ it to evaluate the surface normal performance of our proposed model. ScanNet dataset is divided into 189916 for training and 20942 for test with file lists provided in [24].

B. Evaluation Metrics

Evaluation Protocol on Monocular Depth Estimation. Following the standard evaluation protocol as in previous works [25], [6], [26], the following quantitative evaluation metrics are adopted in our experiments:

- Abs relative error (abs-rel): $\frac{1}{K}\sum_{i=1}^{K}\frac{|\tilde{d}_i - d_i^\star|}{d_i^\star}$;
- Squared Relative difference (sq-rel): $\frac{1}{K}\sum_{i=1}^{K}\frac{||\tilde{d}_i - d_i^\star||^2}{d_i^\star}$;
- root mean squared error (rms): $\sqrt{\frac{1}{K}\sum_{i=1}^{K}(\tilde{d}_i - d_i^\star)^2}$;
- mean log10 error (log-rms): $\sqrt{\frac{1}{K}\sum_{i=1}^{K}\|\log_{10}(\tilde{d}_i) - \log_{10}(d_i^\star)\|^2}$;
- accuracy with threshold t: percentage (%) of $d_i^\star$, subject to $\max(\frac{d_i^\star}{\tilde{d}_i}, \frac{\tilde{d}_i}{d_i^\star}) = \delta < t$ $(t \in [1.25, 1.25^2, 1.25^3])$.

Where $\tilde{d}_i$ and $d_i^\star$ is the ground-truth depth and the estimated depth at pixel i respectively; K is the total number of pixels of the test images.

Evaluation Protocol on Semantic Segmentation. As for semantic segmentation, we consider two metrics [69], [10], *i.e.* pixel accuracy (pixAcc) and mean intersection over union (mIoU), averaged over classes. The normal prediction performance is evaluated with five metrics. We compute the per-pixel angle distance between prediction and ground-truth, then compute mean and median for valid pixels with given ground-truth normal.

Evaluation Protocol on Surface Normal Estimation. For the evaluation of surface normal estimation, we utilize five standard evaluation metrics [70], *i.e.* mean and median angle distance between prediction and ground-truth for valid pixels, and the fraction of pixels with angle difference with ground-truth less than t $(t \in [11.25°, 22.5°, 30°]$.

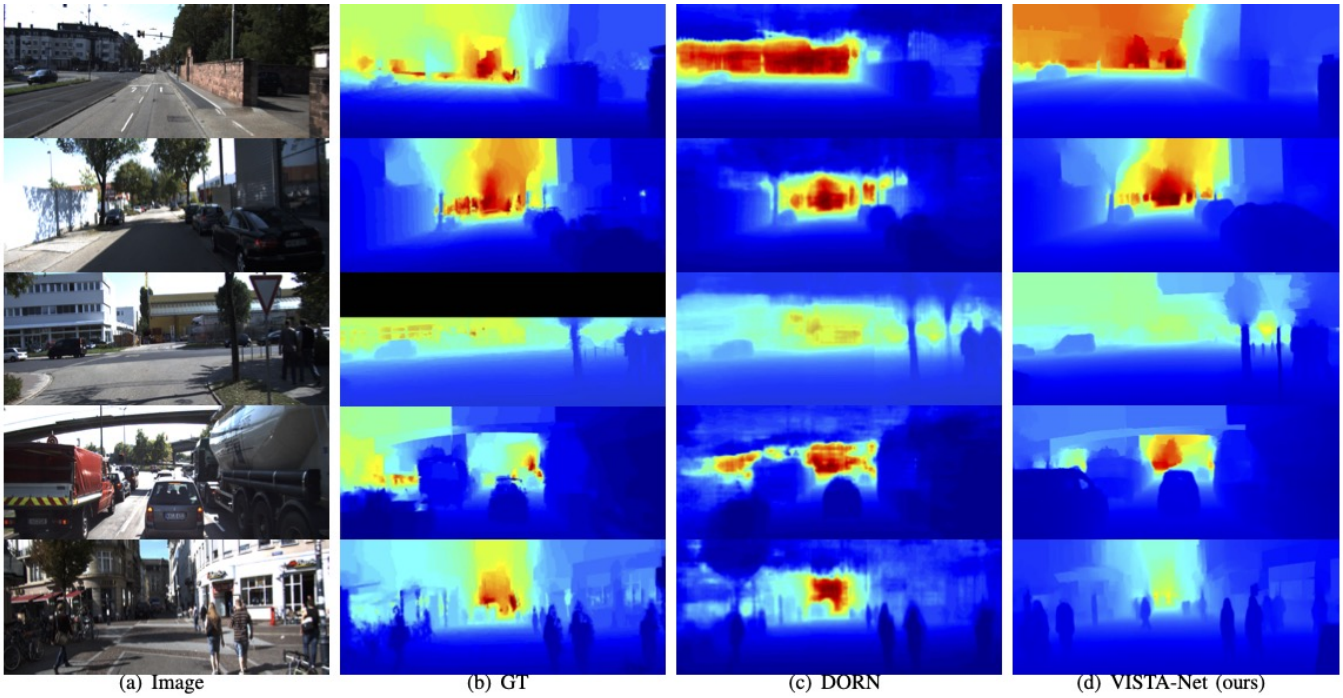

(a) Image (b) GT (c) DORN (d) VISTA-Net (ours)

Fig. 3: Qualitative examples on KITTI dataset.

TABLE I: Depth Estimation: KITTI dataset. Only monocular estimation methods are reported.

Method	Error (lower is better)				Accuracy (higher is better)		
	abs-rel	sq-rel	rms	log-rms	$\delta < 1.25$	$\delta < 1.25^2$	$\delta < 1.25^3$
CC [60]	0.140	1.070	5.326	0.217	0.826	0.941	0.975
Bian *et al.*[61]	0.137	1.089	5.439	0.217	0.830	0.942	0.975
S^3Net [62]	0.124	0.826	4.981	0.200	0.846	0.955	0.982
MS-CRF [32]	0.125	0.899	4.685	-	0.816	0.951	0.983
AG-CRF [5]	0.126	0.901	4.689	0.157	0.813	0.950	0.982
DeFeat [63]	0.126	0.925	5.035	0.200	0.862	0.954	0.980
Monodepth2 [64]	0.115	0.903	4.863	0.193	0.877	0.959	0.981
pRGBD [65]	0.113	0.793	4.655	0.188	0.874	0.960	0.983
SGDepth [66]	0.107	0.768	4.468	0.180	0.891	0.963	0.982
Johnston *et al.*[13]	0.106	0.861	4.699	0.185	0.889	0.962	0.982
Shu *et al.*[67]	0.104	0.729	4.481	0.179	0.893	0.965	0.984
DORN [28]	0.072	0.307	2.727	0.120	0.932	0.984	0.994
Yin *et al.*[68]	0.072	-	3.258	0.117	0.938	0.990	**0.998**
PackNet-SfM [31]	0.071	0.359	3.153	0.109	0.944	0.990	0.997
PGA-Net [17]	0.063	0.267	2.634	0.101	0.952	0.992	**0.998**
Lee *et al.*[30]	**0.061**	0.261	2.834	0.099	0.954	0.992	**0.998**
VISTA-Net (ours)	**0.061**	**0.211**	**2.445**	**0.092**	**0.960**	**0.994**	**0.998**

C. Implementation Details

The proposed VISTA-Net is implemented in *Pytorch*. The experiments are conducted on four Nvidia Quadro RTX 6000 GPUs, each with 24 GB memory. The ResNet-101 architecture pretrained on ImageNet [71] is considered in the experiments for initializing the backbone network of VISTA-Net. Our model can be used for effective deep feature learning in multi-scale contexts. To boost the performance, following previous works [72], [5], we also consider multi-features produced from different convolutional blocks of a backbone CNN (*e.g.* res3c, ref4f, ref5d of a ResNet-50).

For the semantic segmentation task, we use a learning rate of 0.001 with a momentum of 0.9 and a weight decay of 0.0001 using a polynomial learning rate scheduler as previously done in [10], [34]. For the the monocular depth estimation task, the learning rate is set to 10^{-4} with weight decay of 0.01. The Adam optimizer is used in all our experiments with a batch size of 8 for monocular depth estimation and 16 for semantic segmentation and surface normal. The total training epochs are set to 50 for depth prediction, to 150 for semantic segmentation, 20 for surface normal and to 500 for the Cityscapes dataset. The default value of T rank is 1 in all tasks.

D. Experimental Results and Analysis

Monocular Depth Estimation. Comparative results on KITTI dataset are shown in Table I. We propose a comparison with state of the art models such as [6], [60], [61], [64], [28], [68], [30], [31], [17]. In addition we demonstrate the effectiveness of our VISTA-Net comparing with MS-CRF [32], a previous

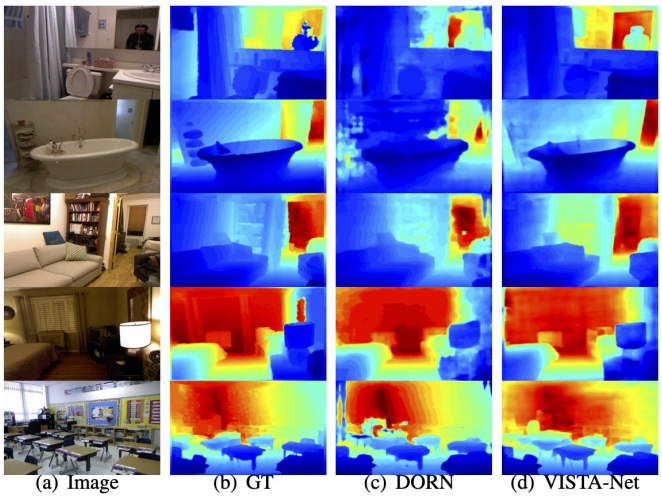

Fig. 4: Qualitative examples on NYU dataset.

TABLE II: Depth Estimation: NYU dataset.

Method	Error (lower is better)			Accuracy (higher is better)		
	rel	log10	rms	$\delta < 1.25$	$\delta < 1.25^2$	$\delta < 1.25^3$
PAD-Net [45]	0.214	0.091	0.792	0.643	0.902	0.977
Li *et al.* [73]	0.152	0.064	0.611	0.789	0.955	0.988
CLIFFNet [74]	0.128	0.171	0.493	0.844	0.964	0.991
Laina *et al.*[27]	0.127	0.055	0.573	0.811	0.953	0.988
MS-CRF [32]	0.121	0.052	0.586	0.811	0.954	0.987
Lee *et al.*[75]	0.119	0.050	-	0.870	0.974	0.993
AG-CRF [5]	0.112	0.051	0.526	0.818	0.960	0.989
DORN [28]	0.115	0.051	0.509	0.828	0.965	0.992
Xia *et al.*[76]	0.116	-	0.512	0.861	0.969	0.991
Yin *et al.*[68]	**0.108**	**0.048**	0.416	0.875	0.976	0.994
Lee *et al.*[30]	0.113	0.049	0.407	0.871	0.977	0.995
VISTA-Net (ours)	0.111	**0.048**	**0.393**	**0.881**	**0.979**	**0.996**

approach which exploit a probabilistic framework for multi-scale feature learning but does not consider an attention mechanisms. Our approach is superior, thus demonstrating the effectiveness of the proposed structured attention model. We also compare with AG-CRF [5] and PGA-Net [17]. Also in this case VISTA-Net outperforms the competitors confirming the importance of having a joint structured spatial- and channel-wise attention model. Note that AG-CRF [5], PGA-Net [17] and VISTA-Net are compared using the same backbone. In order to demonstrate the competitiveness of our approach in an indoor scenario we also report the results on NYUD-V2 dataset in Table II. Similarly to the experiments on KITTI, VISTA-Net outperforms both state of the art approaches and previous methods based on attention gates and CRFs [32], [5]. In Fig. 3 is shown a qualitative comparison of our method with DORN [28]. Results indicate that VISTA-Net generates better depth maps, in particular one can appreciate the opening of the sky and the smoothness of the prediction on the sides. Fig. 4 shows a similar comparison done on NYU dataset. The same accuracy in the prediction is visible also in this case, objects are more distinguishable w.r.t. DORN (e.g. the bathtub in row 2 and the desks in row 5).

Semantic Segmentation. We first compare VISTA-Net with the most recent methods on the Pascal-Context dataset, including [10], [2], [82], [83], [84], [81], [37], [9], [12], [17]. VISTA-Net, as shown in Table III, is 0.3 points better according to

Fig. 5: Qualitative examples on the Pascal-Context dataset.

TABLE III: Semantic Segmentation: PASCAL-Context. D-ResNet-101 denotes Dilated ResNet-101.

Method	Backbone	pixAcc%	mIoU%
CFM (VGG+MCG) [77]	VGG-16	-	34.4
DeepLab-v2 [34]	VGG-16	-	37.6
FCN-8s [33]	VGG-16	50.7	37.8
BoxSup [78]	VGG-16	-	40.5
ConvPP-8s [79]	VGG-16	-	41.0
PixelNet [80]	VGG-16	51.5	41.4
HRNetV2 [81]	-	-	54.0
EncNet [10]	D-ResNet-101	79.23	51.7
DANet [2]	D-ResNet-101	-	52.6
ANN [82]	D-ResNet-101	-	52.8
SpyGR [12]	ResNet-101	-	52.8
SANet [9]	ResNet-101	80.6	53.0
SVCNet [83]	ResNet-101	-	53.2
CFNet [84]	ResNet-101	-	54.0
APCNet [37]	D-ResNet-101	-	54.7
PGA-Net [17]	D-ResNet-101	**81.2**	55.1
VISTA-Net (ours)	D-ResNet-101	81.1	**55.4**

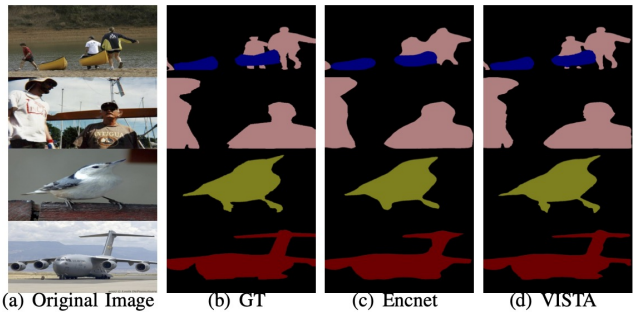

Fig. 6: Qualitative results on the Pascal VOC2012 dataset.

the mIoU metric than the best available method, *i.e.* PGA-

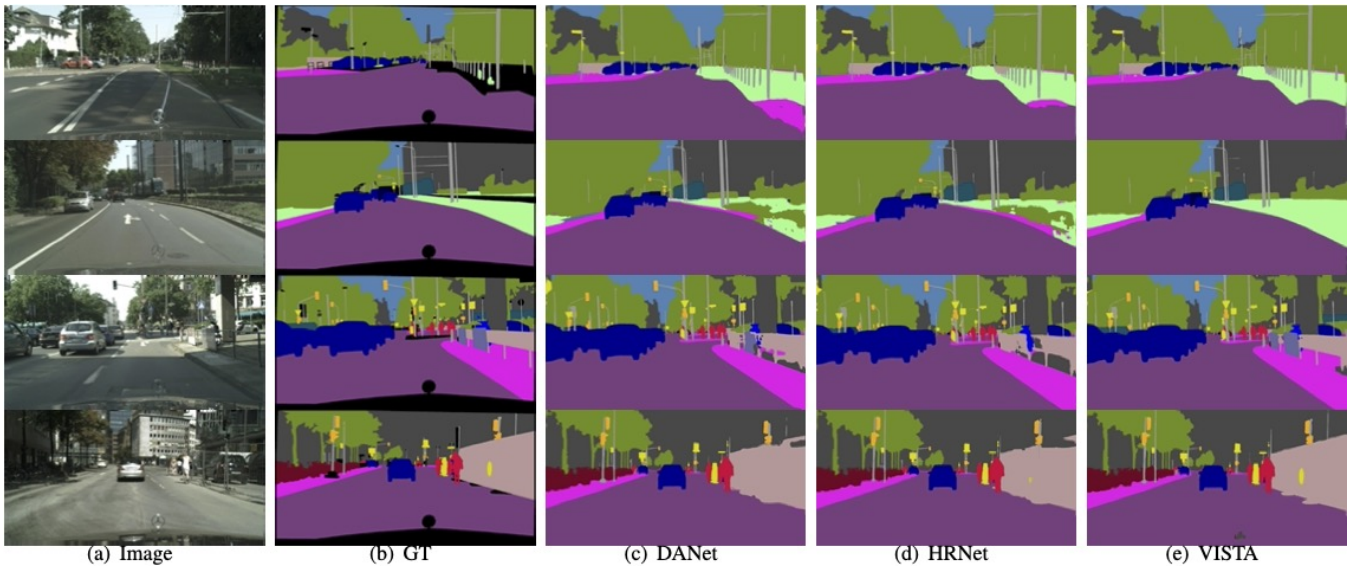

(a) Image (b) GT (c) DANet (d) HRNet (e) VISTA

Fig. 7: Qualitative semantic segmentation results on Cityscapes dataset.

TABLE IV: Semantic Segmentation: PASCAL VOC 2012 validation set. All the methods are tested with multi-scale inputs. $*$ means adopting COCO-pretrained weights.

Method	Backbone	mIoU%
DeepLabV3 [85]	D-ResNet-101	75.7
Dynamic [86]	Layer33	79.0
Res2Net [87]	Res2Net-101	80.2
DANet [2]	ResNet-101	80.4
Auto-Deeplab [88]*	ResNet-101	82.0
EncNet [10]	D-ResNet-101	85.9
SANet [9]*	ResNet-101	86.1
VISTA-Net (ours)	D-ResNet-101	**89.8**

TABLE V: Semantic Segmentation: Cityscapes validation and testing set (trained on the standard training set).

Method	Backbone	Test set	mIoU
Dynamic [86]	Layer33-PSP	Val	79.7
SpyGR [12]	ResNet-101	Val	80.5
CCNet [57]	ResNet-101	Val	81.3
Panoptic-DeepLab [89]	D-ResNet-101	Val	81.5
CDGCNet [90]	D-ResNet-101	Val	81.9
VISTA-Net (ours)	HRNetV2-W48	Val	**82.3**
PSANet [56]	D-ResNet-101	Test	78.6
PAN [91]	D-ResNet-101	Test	78.6
AAF [92]	D-ResNet-101	Test	79.1
HRNet [81]	HRNetV2-W48	Test	80.4
Dynamic [86]	Layer33-PSP	Test	80.7
VISTA-Net (ours)	HRNetV2-W48	Test	**81.4**

net. Importantly, VISTA-Net outperforms EncNet [10], which uses only channel-wise attention, as well as DANet [2], which considers separate spatial and channel attention models. Meanwhile, the visualisation result is shown in Fig. 5.

We also compare our method with state of the art methods on PASCAL VOC2012, including [85], [86], [87], [2], [88], [10], [9], [98]. Unsurprisingly, our method not only outperforms single channel attention methods like EncNet [10] and single spatial attention methods like SANet [9] but also DANet [2] which considers separate spatial and channel attention models. VISTA-Net, as shown in Table IV, is 3.7 points better according to the mIoU metric than the best available method, *i.e.* SANet. This clearly confirms the advantage of our probabilistic formulation and the importance of handling the spatial and channel wise attention in a structured manner within an unified probabilistic framework.

Meanwhile, the visualisation result is shown in Fig. 6. In

TABLE VI: Semantic segmentation: Cityscapes test set (learned on the train+val set, multi-scale and flipping). D-ResNet-101 is short for Dilated-ResNet-101.

Method	Backbone	mIoU	iIoU cla	IoU cat.	iIoU cat.
DeepLab [34]	D-ResNet-101	70.4	42.6	86.4	67.7
PADNet [45]	D-ResNet-101	80.3	58.8	90.8	78.5
Dynamic [86]	Layer33-PSP	80.7	-	-	-
SVCNet [83]	ResNet-101	81.0	-	-	-
ANN [82]	D-ResNet-101	81.3	-	-	-
CCNet [57]	D-ResNet-101	81.4	-	-	-
DANet [2]	D-ResNet-101	81.5	-	-	-
DGMN [15]	D-ResNet-101	81.6	-	-	-
SpyGR [12]	ResNet-101	81.6	-	-	-
HRNet [81]	HRNetV2-W48	81.6	61.8	**92.1**	**82.2**
ACFNet [93]	ResNet-101	81.8	-	-	-
DGCNet [58]	ResNet-101	82.0	-	-	-
HANet [94]	ResNext-101	82.1	-	-	-
VISTA-Net (ours)	HRNetV2-W48	**82.2**	**62.7**	91.9	82.1

TABLE VII: Surface normal prediction: ScanNet dataset.

Methods	Error metric		Accuracy metric		
	mean	median	11.25	22.5	30
Skip-Net[95]	26.2	20.6	28.8	54.3	67.0
Zhang*et al.* [96]	23.3	16.0	40.4	63.1	71.9
GeoNet [97]	19.8	11.3	49.7	70.4	77.7
FrameNet [43]	15.3	8.1	60.6	78.6	84.7
VISTA-Net (ours)	**15.1**	**7.5**	**63.8**	**80.0**	**85.2**

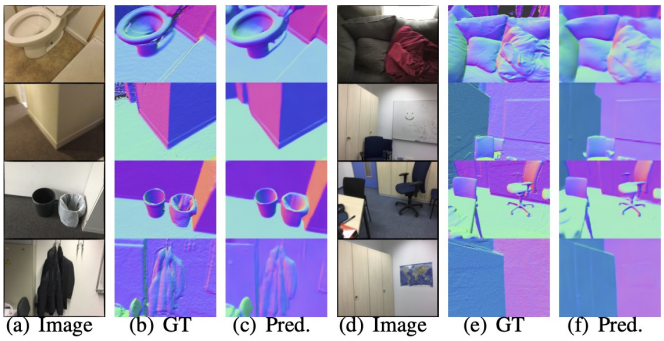

Fig. 8: Qualitative examples on ScanNet dataset.

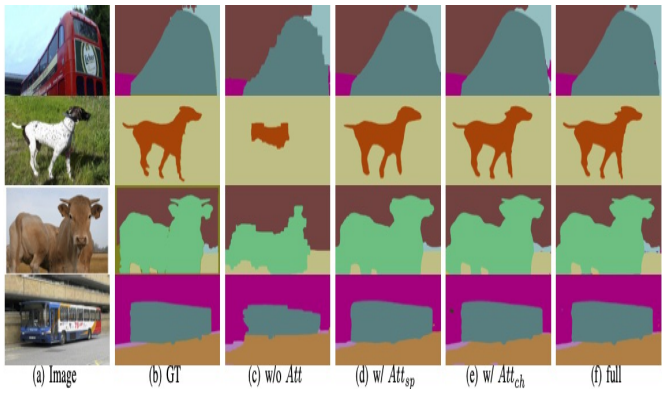

Fig. 9: Comparison of different attention mechanisms of VISTA-Net on Pascal-context dataset.

Table V we report the results of our method on Cityscape val/test dataset. For fair comparison, all methods do not use multi-scale and flipping. According to Table V, VISTA-Net outperforms the competitors of 0.4% and 0.7% mIoU in validation and testing set. According to the visualization results (Fig. 7), our method capture more information about details than DANet and HRNet. For example in the fourth row, our method successfully predicts the yellow warning symbol while DANet and HRNet both miss it. Moreover, we also compare our method with state of the art attention based methods learned on the train+val set with multi-scale and flipping in Table VI, including [45], [86], [83], [82], [57], [2], [15], [12], [81], [93], [58], [94]. We outperform not only DANet and HRNet but also the state-of-the-art approach HANet.

Surface Normal Estimation. We compare VISTA-Net with the state-of-the-art RGB-based methods, including Eigen *et al.* [25], GeoNe [97] and FrameNet [43]. We adapt the publicly available training code and keep their fine-tune and pre-train model. The results shown in Table VII. VISTA-Net outperforms the state-of-the-art on all five metrics. Some samples are shown in Fig. 8 together with the ground-truth.

Ablation Study. We also perform an ablation study on the Pascal-context dataset to further demonstrate each proposed component's impact. Table. VIII shows that the performance of VISTA-Net degrades not only when the model does not employ the structured attention mechanism but also when only channel-wise or spatial-wise attention is used. Moreover, we

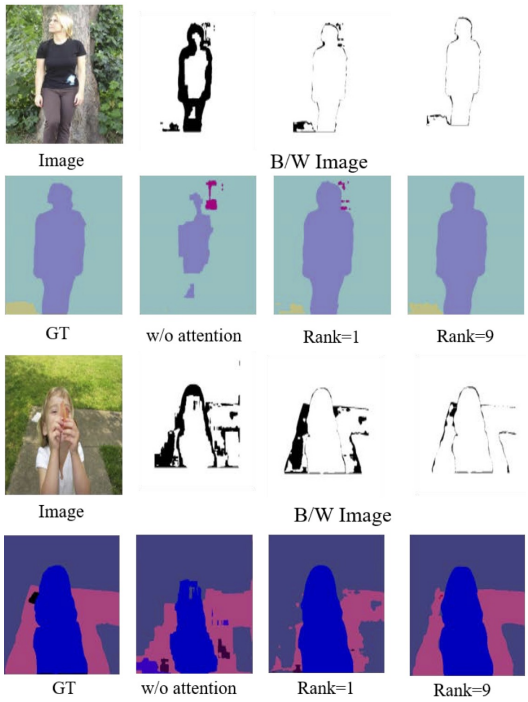

Fig. 10: Comparison of different variations of VISTA-Net on Pascal-context dataset.

TABLE VIII: Ablation study on the Pascal-context dataset: performance of VISTA-Net for differ-ent attention mecha-nisms and scales.

Scales	Structured Attention	Probabilistic	mIoU	PixAcc
DANet [2]	Separate Attention	No	52.6	-
Single scale	No structure	Yes	51.7	78.9
	Spatial	Yes	53.0	79.7
	Channel	Yes	53.1	79.8
	Low-rank tensor	No	53.2	79.9
	High-rank tensor	Yes	53.9	80.3
Multiple scale	No structure	Yes	52.8	79.5
	Spatial	Yes	54.8	80.8
	Channel	Yes	54.6	80.6
	Low-rank tensor	No	54.7	80.7
	High-rank tensor	Yes	**55.4**	**81.1**

can also see the advantage of using the proposed probabilistic formulation for joint modeling both spatial- and channel-wise attention in a principled manner. For the sake of completeness, we also report the results of DANet. Meanwhile, Fig. 9 depicts segmentation maps obtained on the Pascal-Context

TABLE IX: Pascal-context dataset: computational cost analysis for different values of T.

rank	IoU	pixacc	parameters	FPS
0	54.2	80.4	45.80M	1.106
1	54.6	80.7	49.85M	1.075
3	54.8	80.8	52.68M	1.011
5	54.5	80.4	54.89M	1.068
7	55.3	81.1	56.79M	0.957
9	55.4	81.1	58.85M	0.868

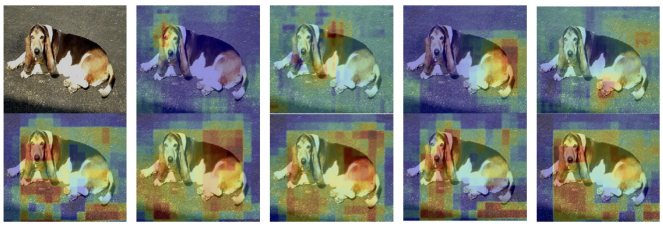

Fig. 11: Attention map visualisation on Pascal context dataset. First row: original image and four channels (slices) of the structured attention tensor $\mathbf{a}$, see (1). Second row, the $T = 5$ attention maps $\mathbf{m}^t$, $t = 1, \ldots, 5$.

dataset using different versions of our method. In particular, we visualize (c) VISTA-Net w/o attention, (d) VISTA-Net w/o Spatial Attention, (e) VISTA-Net w/o Channel Attention, and (f) VISTA-Net (full model). From left to right, the results become more similar to the ground truth, indicating our proposed attention model's clear advantage. Interestingly, the performance achieved in each of the variants (spatial, channel) is similar. This leads us to believe that the proposed method's competitive advantage is combining structured attention with a probabilistic formulation. Notably, the feature refinement through message passing seems to be the most crucial contribution to improving performance. In Table. IX we show the results of our experiments in order to analyze the computational cost of our method. In particular, we perform an analysis on the Pascal-context dataset and at varying T. In the table IX, FPS means Frames Per Second. As expected, when the rank increases, we also observe an increase in parameters and a reduction in speed. Finally, in Fig. 10 we propose a few qualitative results compared with their B/W images on the Pascal-context dataset. It is shown the importance of the attention model, and the result obtained increasing the iterations. In the odd rows are shown the misclassified pixels (in black). The image shows clearly how the proposed iterative approach based on message passing is beneficial for the final prediction.

Fig. 11 shows different visualizations regarding the learned structured attention on an image from the Pascal-Context dataset. The first row shows the original image, together with four slices (channels) of the overall structured attention tensor $\mathbf{a}$ as defined in (1). The second row shows the $T = 5$ spatial maps of the structured tensor $\mathbf{m}^t$. While the latter seem to be spread all along the dog's body with different shapes, we observe that by optimally combining the $\mathbf{m}^t$ and the $\mathbf{v}^t$, different slices of the final structured attention tensor are able to focus on different important parts of the dog: the head, the body, the tail and the rear paws, thus allowing to take much more accurate pixel-level predictions for segmentation. We also provide the computed attention maps on some sample images in KITTI dataset in Fig. 12. As expected, the final structured attention tensors manage to capture important information among different depths. For example, in the fourth row, structured attention focus on farthest frost, middle jungle, and close road. Fig. 12 proves that different structured attention tensor $\mathbf{a}$ can capture distinct and

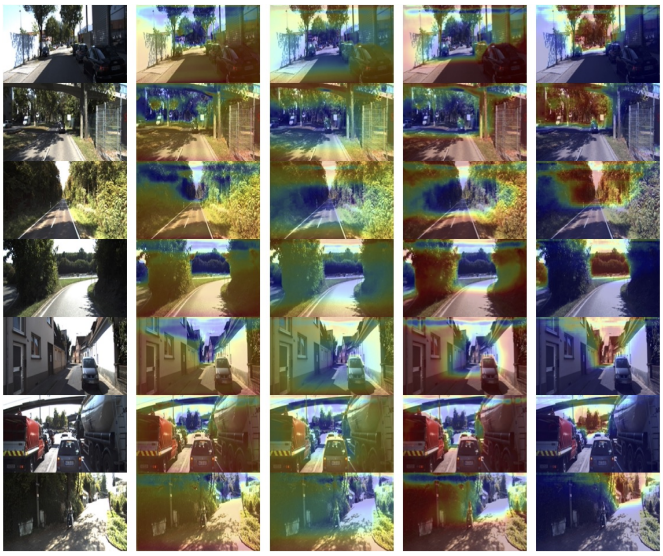

Fig. 12: Qualitative structured attention examples of monocular depth prediction on the KITTI raw dataset. First column is original image and next four columns is structured attention, defined by (1).

representative semantic information due to the combination of both channel- and spatial-wise attention.

V. Conclusions

In this paper we proposed a novel approach to improve the learning of deep features representations for dense pixel-wise prediction tasks. Our approach seamlessly integrates a novel structured attention model within a probabilistic framework. In particular, we proposed to structure the attention tensors as the sum of T rank tensors, each being the tensor-product of a spatial attention map and a channel attention vector. These two kinds of variables are jointly learned within the probabilistic formulation made tractable thanks to the variational approximation. The proposed structured attention is rich enough to capture complex spatial- and channel-level interdependencies, while being efficient to compute. The overall optimisation of the probabilistic model and of the CNN front-end is performed jointly. Extensive experimental evaluations show that VISTA-Net outperforms state-of-the-art methods on several datasets, thus confirming the importance of jointly structuring the spatial- and channel-wise attention variables for learning effective deep representations for dense pixel-level prediction tasks. Future works include the exploration of the proposed variational structured attention networks for geometry-aware representation learning with uncertainty [99] and generative scene modelling [100], [101], [102].

References

[1] L.-C. Chen, Y. Yang, J. Wang, W. Xu, and A. L. Yuille, "Attention to scale: Scale-aware semantic image segmentation," in *CVPR*, 2016. 1, 3

[2] J. Fu, J. Liu, H. Tian, Y. Li, Y. Bao, Z. Fang, and H. Lu, "Dual attention network for scene segmentation," in *CVPR*, 2019. 1, 2, 3, 4, 8, 9, 10

[3] F. Liu, C. Shen, and G. Lin, "Deep convolutional neural fields for depth estimation from a single image," in *CVPR*, 2015. 1, 2

[4] A. Roy and S. Todorovic, "Monocular depth estimation using neural regression forest," in *CVPR*, 2016. 1, 2

[5] D. Xu, W. Ouyang, X. Alameda-Pineda, E. Ricci, X. Wang, and N. Sebe, "Learning deep structured multi-scale features using attention-gated crfs for contour prediction," in *NeurIPS*, 2017. 1, 3, 5, 7, 8

[6] D. Eigen, C. Puhrsch, and R. Fergus, "Depth map prediction from a single image using a multi-scale deep network," in *NeurIPS*, 2014. 1, 2, 6, 7

[7] V. Mnih, N. Heess, A. Graves *et al.*, "Recurrent models of visual attention," in *NeurIPS*, 2014. 1

[8] H. Zhan, R. Garg, C. Saroj Weerasekera, K. Li, H. Agarwal, and I. Reid, "Unsupervised learning of monocular depth estimation and visual odometry with deep feature reconstruction," in *CVPR*, 2018, pp. 340–349. 1

[9] Z. Zhong, Z. Q. Lin, R. Bidart, X. Hu, I. B. Daya, Z. Li, W.-S. Zheng, J. Li, and A. Wong, "Squeeze-and-attention networks for semantic segmentation," in *CVPR*, 2020, pp. 13 065–13 074. 1, 3, 6, 8, 9

[10] H. Zhang, K. Dana, J. Shi, Z. Zhang, X. Wang, A. Tyagi, and A. Agrawal, "Context encoding for semantic segmentation," in *CVPR*, 2018. 1, 3, 6, 7, 8, 9

[11] X. Song, Y. Dai, D. Zhou, L. Liu, W. Li, H. Li, and R. Yang, "Channel attention based iterative residual learning for depth map super-resolution," in *CVPR*, 2020, pp. 5631–5640. 1

[12] X. Li, Y. Yang, Q. Zhao, T. Shen, Z. Lin, and H. Liu, "Spatial pyramid based graph reasoning for semantic segmentation," in *CVPR*, 2020, pp. 8950–8959. 1, 8, 9, 10

[13] A. Johnston and G. Carneiro, "Self-supervised monocular trained depth estimation using self-attention and discrete disparity volume," in *CVPR*, 2020, pp. 4756–4765. 1, 7

[14] C.-P. Tay, S. Roy, and K.-H. Yap, "Aanet: Attribute attention network for person re-identifications," in *CVPR*, 2019, pp. 7134–7143. 1

[15] L. Zhang, D. Xu, A. Arnab, and P. H. Torr, "Dynamic graph message passing networks," in *CVPR*, 2020, pp. 3726–3735. 1, 3, 9, 10

[16] Y. Chen, M. Rohrbach, Z. Yan, Y. Shuicheng, J. Feng, and Y. Kalantidis, "Graph-based global reasoning networks," in *CVPR*, 2019. 1, 3

[17] D. Xu, X. Alameda-Pineda, W. Ouyang, E. Ricci, X. Wang, and N. Sebe, "Probabilistic graph attention network with conditional kernels for pixel-wise prediction," *TPAMI*, 2020. 1, 2, 3, 7, 8

[18] T. Minka and J. Winn, "Gates," in *NeurIPS*, 2009. 1

[19] N. Silberman, D. Hoiem, P. Kohli, and R. Fergus, "Indoor segmentation and support inference from rgbd images," in *ECCV*, 2012. 2, 6

[20] A. Geiger, P. Lenz, C. Stiller, and R. Urtasun, "Vision meets robotics: The kitti dataset," *IJRR*, 2013. 2, 6

[21] R. Mottaghi, X. Chen, X. Liu, N.-G. Cho, S.-W. Lee, S. Fidler, R. Urtasun, and A. Yuille, "The role of context for object detection and semantic segmentation in the wild," in *CVPR*, 2014. 2, 6

[22] M. Everingham, L. Van Gool, C. K. Williams, J. Winn, and A. Zisserman, "The pascal visual object classes (voc) challenge," *IJCV*, vol. 88, no. 2, pp. 303–338, 2010. 2, 6

[23] M. Cordts, M. Omran, S. Ramos, T. Rehfeld, M. Enzweiler, R. Benenson, U. Franke, S. Roth, and B. Schiele, "The cityscapes dataset for semantic urban scene understanding," in *CVPR*, 2016. 2, 6

[24] A. Dai, A. X. Chang, M. Savva, M. Halber, T. Funkhouser, and M. Nießner, "Scannet: Richly-annotated 3d reconstructions of indoor scenes," in *CVPR*, 2017, pp. 5828–5839. 2, 6

[25] D. Eigen and R. Fergus, "Predicting depth, surface normals and semantic labels with a common multi-scale convolutional architecture," in *ICCV*, 2015. 2, 6, 10

[26] P. Wang, X. Shen, Z. Lin, S. Cohen, B. Price, and A. Yuille, "Towards unified depth and semantic prediction from a single image," in *CVPR*, 2015. 2, 6

[27] I. Laina, C. Rupprecht, V. Belagiannis, F. Tombari, and N. Navab, "Deeper depth prediction with fully convolutional residual networks," *arXiv preprint arXiv:1606.00373*, 2016. 2, 8

[28] H. Fu, M. Gong, C. Wang, K. Batmanghelich, and D. Tao, "Deep ordinal regression network for monocular depth estimation," in *CVPR*, 2018. 2, 3, 7, 8

[29] Y. Gan, X. Xu, W. Sun, and L. Lin, "Monocular depth estimation with affinity, vertical pooling, and label enhancement," in *ECCV*, 2018, pp. 224–239. 2

[30] J. H. Lee, M.-K. Han, D. W. Ko, and I. H. Suh, "From big to small: Multi-scale local planar guidance for monocular depth estimation," *arXiv preprint arXiv:1907.10326*, 2019. 2, 7, 8

[31] V. Guizilini, R. Ambrus, S. Pillai, A. Raventos, and A. Gaidon, "3d packing for self-supervised monocular depth estimation," in *CVPR*, 2020, pp. 2485–2494. 2, 7

[32] D. Xu, E. Ricci, W. Ouyang, X. Wang, and N. Sebe, "Multi-scale continuous crfs as sequential deep networks for monocular depth estimation," in *CVPR*, 2017. 2, 3, 6, 7, 8

[33] J. Long, E. Shelhamer, and T. Darrell, "Fully convolutional networks for semantic segmentation," in *CVPR*, 2015. 2, 6, 8

[34] L.-C. Chen, G. Papandreou, I. Kokkinos, K. Murphy, and A. L. Yuille, "Deeplab: Semantic image segmentation with deep convolutional nets, atrous convolution, and fully connected crfs," *arXiv preprint arXiv:1606.00915*, 2016. 2, 3, 6, 7, 8, 9

[35] F. Yu and V. Koltun, "Multi-scale context aggregation by dilated convolutions," *arXiv preprint arXiv:1511.07122*, 2015. 2

[36] Y. Yuan and J. Wang, "Ocnet: Object context network for scene parsing," *arXiv preprint arXiv:1809.00916*, 2018. 2

[37] J. He, Z. Deng, L. Zhou, Y. Wang, and Y. Qiao, "Adaptive pyramid context network for semantic segmentation," in *CVPR*, 2019. 2, 8

[38] H. Noh, S. Hong, and B. Han, "Learning deconvolution network for semantic segmentation," in *ICCV*, 2015. 2

[39] V. Badrinarayanan, A. Handa, and R. Cipolla, "Segnet: A deep convolutional encoder-decoder architecture for robust semantic pixel-wise labelling," *arXiv preprint arXiv:1505.07293*, 2015. 2

[40] Z. Liu, X. Li, P. Luo, C.-C. Loy, and X. Tang, "Semantic image segmentation via deep parsing network," in *ICCV*, 2015. 3

[41] A. Arnab, S. Jayasumana, S. Zheng, and P. H. Torr, "Higher order conditional random fields in deep neural networks," in *ECCV*. Springer, 2016. 3

[42] S. Zheng, S. Jayasumana, B. Romera-Paredes, V. Vineet, Z. Su, D. Du, C. Huang, and P. H. Torr, "Conditional random fields as recurrent neural networks," in *ICCV*, 2015. 3

[43] J. Huang, Y. Zhou, T. Funkhouser, and L. J. Guibas, "Framenet: Learning local canonical frames of 3d surfaces from a single rgb image," in *Proceedings of the IEEE International Conference on Computer Vision*, 2019, pp. 8638–8647. 3, 9, 10

[44] W. Xian, Z. Li, M. Fisher, J. Eisenmann, E. Shechtman, and N. Snavely, "Uprightnet: geometry-aware camera orientation estimation from single images," in *ICCV*, 2019, pp. 9974–9983. 3

[45] D. Xu, W. Ouyang, X. Wang, and N. Sebe, "Pad-net: Multi-tasks guided prediction-and-distillation network for simultaneous depth estimation and scene parsing," in *CVPR*, 2018. 3, 8, 9, 10

[46] Z. Zhang, Z. Cui, C. Xu, Z. Jie, X. Li, and J. Yang, "Joint task-recursive learning for semantic segmentation and depth estimation," in *ECCV*, 2018, pp. 235–251. 3

[47] Z. Zhang, Z. Cui, C. Xu, Y. Yan, N. Sebe, and J. Yang, "Pattern-affinitive propagation across depth, surface normal and semantic segmentation," in *CVPR*, 2019, pp. 4106–4115. 3

[48] D. Xu, W. Wang, H. Tang, H. Liu, N. Sebe, and E. Ricci, "Structured attention guided convolutional neural fields for monocular depth estimation," in *CVPR*, 2018. 3

[49] S. Vandenhende, S. Georgoulis, and L. Van Gool, "Mti-net: Multi-scale task interaction networks for multi-task learning," *ECCV*, 2020. 3

[50] Y. Xu, D. Xu, X. Hong, W. Ouyang, R. Ji, and G. Zhao, "Structured modeling of joint deep feature and prediction refinement for salient object detection," in *ICCV*, 2019. 3

[51] T. Xiao, Y. Xu, K. Yang, J. Zhang, Y. Peng, and Z. Zhang, "The application of two-level attention models in deep convolutional neural network for fine-grained image classification," in *CVPR*, 2015. 3

[52] J. K. Chorowski, D. Bahdanau, D. Serdyuk, K. Cho, and Y. Bengio, "Attention-based models for speech recognition," in *NeurIPS*, 2015. 3

[53] A. Vaswani, N. Shazeer, N. Parmar, J. Uszkoreit, L. Jones, A. N. Gomez, Ł. Kaiser, and I. Polosukhin, "Attention is all you need," in *NIPS*, 2017. 3

[54] Y. Kim, C. Denton, L. Hoang, and A. M. Rush, "Structured attention networks," in *ICLR*, 2017. 3

[55] M.-T. Luong, H. Pham, and C. D. Manning, "Effective approaches to attention-based neural machine translation," in *EMNLP*, 2015. 3

[56] H. Zhao, Y. Zhang, S. Liu, J. Shi, C. Change Loy, D. Lin, and J. Jia, "Psanet: Point-wise spatial attention network for scene parsing," in *ECCV*, 2018. 3, 9

[57] Z. Huang, X. Wang, L. Huang, C. Huang, Y. Wei, and W. Liu, "Ccnet: Criss-cross attention for semantic segmentation," in *Proceedings of the IEEE International Conference on Computer Vision*, 2019, pp. 603–612. 3, 9, 10

[58] L. Zhang, X. Li, A. Arnab, K. Yang, Y. Tong, and P. H. Torr, "Dual graph convolutional network for semantic segmentation," *arXiv preprint arXiv:1909.06121*, 2019. 3, 9, 10

[59] D. Xu, W. Ouyang, E. Ricci, X. Wang, and N. Sebe, "Learning cross-modal deep representations for robust pedestrian detection," in *CVPR*, 2017. 3

[60] A. Ranjan, V. Jampani, L. Balles, K. Kim, D. Sun, J. Wulff, and M. J. Black, "Competitive collaboration: Joint unsupervised learning of depth, camera motion, optical flow and motion segmentation," in *CVPR*, 2019. 7

[61] J. Bian, Z. Li, N. Wang, H. Zhan, C. Shen, M.-M. Cheng, and I. Reid, "Unsupervised scale-consistent depth and ego-motion learning from monocular video," in *NeurIPS*, 2019. 7

[62] B. Cheng, I. S. Saggu, R. Shah, G. Bansal, and D. Bharadia, "s^3 net: Semantic-aware self-supervised depth estimation with monocular videos and synthetic data," *ECCV*, 2020. 7

[63] J. Spencer, R. Bowden, and S. Hadfield, "Defeat-net: General monocular depth via simultaneous unsupervised representation learning," in *CVPR*, 2020, pp. 14 402–14 413. 7

[64] C. Godard, O. Mac Aodha, M. Firman, and G. J. Brostow, "Digging into self-supervised monocular depth estimation," in *ICCV*, 2019. 7

[65] L. Tiwari, P. Ji, Q.-H. Tran, B. Zhuang, S. Anand, and M. Chandraker, "Pseudo rgb-d for self-improving monocular slam and depth prediction," *ECCV*, 2020. 7

[66] M. Klingner, J.-A. Termöhlen, J. Mikolajczyk, and T. Fingscheidt, "Self-supervised monocular depth estimation: Solving the dynamic object problem by semantic guidance," *ECCV*, 2020. 7

[67] C. Shu, K. Yu, Z. Duan, and K. Yang, "Feature-metric loss for self-supervised learning of depth and egomotion," *ECCV*, 2020. 7

[68] W. Yin, Y. Liu, C. Shen, and Y. Yan, "Enforcing geometric constraints of virtual normal for depth prediction," in *ICCV*, 2019. 7, 8

[69] B. Zhou, H. Zhao, X. Puig, S. Fidler, A. Barriuso, and A. Torralba, "Scene parsing through ade20k dataset," in *CVPR*, 2017. 6

[70] D. F. Fouhey, A. Gupta, and M. Hebert, "Data-driven 3d primitives for single image understanding," in *ICCV*, 2013. 6

[71] J. Deng, W. Dong, R. Socher, L.-J. Li, K. Li, and L. Fei-Fei, "Imagenet: A large-scale hierarchical image database," in *CVPR*, 2009. 7

[72] S. Xie and Z. Tu, "Holistically-nested edge detection," in *ICCV*, 2015. 7

[73] J. Li, R. Klein, and A. Yao, "A two-streamed network for estimating fine-scaled depth maps from single rgb images," in *ICCV*, 2017. 8

[74] W. Lijun, Z. Jianming, W. Yifan, L. Huchuan, and R. Xiang, "Cliffnet for monocular depth estimation with hierarchical embedding loss," *ECCV*, 2020. 8

[75] J.-H. Lee and C.-S. Kim, "Multi-loss rebalancing algorithm for monocular depth estimation," *ECCV*, 2020. 8

[76] Z. Xia, P. Sullivan, and A. Chakrabarti, "Generating and exploiting probabilistic monocular depth estimates," in *CVPR*, 2020, pp. 65–74. 8

[77] J. Dai, K. He, and J. Sun, "Convolutional feature masking for joint object and stuff segmentation," in *CVPR*, 2015. 8

[78] ——, "Boxsup: Exploiting bounding boxes to supervise convolutional networks for semantic segmentation," in *ICCV*, 2015. 8

[79] S. Xie, X. Huang, and Z. Tu, "Top-down learning for structured labeling with convolutional pseudoprior," in *ECCV*. Springer, 2016. 8

[80] A. Bansal, X. Chen, B. Russell, A. Gupta, and D. Ramanan, "Pixelnet: Representation of the pixels, by the pixels, and for the pixels," *arXiv preprint arXiv:1702.06506*, 2017. 8

[81] J. Wang, K. Sun, T. Cheng, B. Jiang, C. Deng, Y. Zhao, D. Liu, Y. Mu, M. Tan, X. Wang *et al.*, "Deep high-resolution representation learning for visual recognition," *TPAMI*, 2020. 8, 9, 10

[82] Z. Zhu, M. Xu, S. Bai, T. Huang, and X. Bai, "Asymmetric non-local neural networks for semantic segmentation," in *ICCV*, 2019. 8, 9, 10

[83] H. Ding, X. Jiang, B. Shuai, A. Q. Liu, and G. Wang, "Semantic correlation promoted shape-variant context for segmentation," in *CVPR*, 2019. 8, 9, 10

[84] H. Zhang, H. Zhang, C. Wang, and J. Xie, "Co-occurrent features in semantic segmentation," in *CVPR*, 2019. 8

[85] L.-C. Chen, G. Papandreou, F. Schroff, and H. Adam, "Rethinking atrous convolution for semantic image segmentation," *arXiv preprint arXiv:1706.05587*, 2017. 9

[86] Y. Li, L. Song, Y. Chen, Z. Li, X. Zhang, X. Wang, and J. Sun, "Learning dynamic routing for semantic segmentation," in *CVPR*, 2020, pp. 8553–8562. 9, 10

[87] S. Gao, M.-M. Cheng, K. Zhao, X.-Y. Zhang, M.-H. Yang, and P. H. Torr, "Res2net: A new multi-scale backbone architecture," *TPAMI*, 2019. 9

[88] C. Liu, L.-C. Chen, F. Schroff, H. Adam, W. Hua, A. L. Yuille, and L. Fei-Fei, "Auto-deeplab: Hierarchical neural architecture search for semantic image segmentation," in *CVPR*, 2019, pp. 82–92. 9

[89] B. Cheng, M. D. Collins, Y. Zhu, T. Liu, T. S. Huang, H. Adam, and L.-C. Chen, "Panoptic-deeplab: A simple, strong, and fast baseline for bottom-up panoptic segmentation," in *CVPR*, 2020, pp. 12 475–12 485. 9

[90] H. Hu, D. Ji, W. Gan, S. Bai, W. Wu, and J. Yan, "Class-wise dynamic graph convolution for semantic segmentation," *ECCV*, 2020. 9

[91] H. Li, P. Xiong, J. An, and L. Wang, "Pyramid attention network for semantic segmentation," *arXiv preprint arXiv:1805.10180*, 2018. 9

[92] T.-W. Ke, J.-J. Hwang, Z. Liu, and S. X. Yu, "Adaptive affinity fields for semantic segmentation," in *Proceedings of the European Conference on Computer Vision (ECCV)*, 2018, pp. 587–602. 9

[93] F. Zhang, Y. Chen, Z. Li, Z. Hong, J. Liu, F. Ma, J. Han, and E. Ding, "Acfnet: Attentional class feature network for semantic segmentation," in *ICCV*, 2019, pp. 6798–6807. 9, 10

[94] S. Choi, J. T. Kim, and J. Choo, "Cars can't fly up in the sky: Improving urban-scene segmentation via height-driven attention networks," in *CVPR*, 2020, pp. 9373–9383. 9, 10

[95] A. Bansal, B. Russell, and A. Gupta, "Marr revisited: 2d-3d alignment via surface normal prediction," in *CVPR*, 2016, pp. 5965–5974. 9

[96] Y. Zhang, S. Song, E. Yumer, M. Savva, J.-Y. Lee, H. Jin, and T. Funkhouser, "Physically-based rendering for indoor scene understanding using convolutional neural networks," in *CVPR*, 2017, pp. 5287–5295. 9

[97] X. Qi, R. Liao, Z. Liu, R. Urtasun, and J. Jia, "Geonet: Geometric neural network for joint depth and surface normal estimation," in *CVPR*, 2018, pp. 283–291. 9, 10

[98] L. Huynh, P. Nguyen-Ha, J. Matas, E. Rahtu, and J. Heikkila, "Guiding monocular depth estimation using depth-attention volume," *ECCV*, 2020. 9

[99] D. Xu, W. Xie, and A. Zisserman, "Geometry-aware video object detection for static cameras," in *BMVC*, 2019. 11

[100] M. Puscas, D. Xu, A. Pilzer, and N. Sebe, "Structured coupled generative adversarial networks for unsupervised monocular depth estimation," in *3DV*, 2019. 11

[101] H. Tang, D. Xu, Y. Yan, H. P. Torr, and N. Sebe, "Local class-specific and global image-level generative adversarial networks for semantic-guided scene generation," in *CVPR*, 2020. 11

[102] T. Park, M.-Y. Liu, T.-C. Wang, and J.-Y. Zhu, "Semantic image synthesis with spatially-adaptive normalization," in *CVPR*, 2019. 11